Quantum entanglement via a controllable four-wave-mixing mechanism in an optomechanical system

Xiang You and Yongmin Li*

State Key Laboratory of Quantum Optics and Quantum Optics Devices, Institute of Opto-Electronics, Shanxi University, Taiyuan 030006, People's Republic of China
and Collaborative Innovation Center of Extreme Optics, Shanxi University, Taiyuan 030006, People's Republic of China

(Received 21 April 2019; published 19 November 2019)

We propose an approach to generate strong quantum entanglement by the controllable four-wave-mixing mechanism in a single-cavity, weak-coupling optomechanical system. The optomechanical system is driven by a strong two-tone pump field and a weak signal field, simultaneously. The two-tone pump field consists of a lower and an upper sideband, which couple with the optical cavity and mechanical resonator, and generate the beam-splitter and two-mode squeezing interactions under the rotating-wave approximation. This interaction mechanism modifies the effective susceptibility of the optomechanical cavity and optomechanically induces a four-wave-mixing process. Strong quantum entanglement can be generated between the signal and four-wave-mixing fields in realistic optomechanical systems. The generation scheme of the quantum entanglement is quite robust against thermal-mechanical noise, and significant entanglement can persist at room temperature in the weak-coupling regime.

DOI: 10.1103/PhysRevA.100.053842

I. INTRODUCTION

Cavity optomechanics explores the interaction between intracavity electromagnetic fields and micromechanical or nanomechanical motion via radiation-pressure force. It provides a powerful platform for fundamental quantum physics, quantum sensing, and quantum information processing [1]. Typical optomechanical first-order interactions include the beam-splitter (BS) and two-mode squeezing (TMS) interactions, which can produce various physical phenomena. The BS interaction enables the exchange between photons and phonons that contribute to sideband cooling [2–7], coherent quantum state transfer, wavelength conversion [8–12], and optomechanically induced transparency [13,14]. In comparison, the TMS interaction enables the generation of photon-phonon pairs, and has been used to realize the entanglement between photons and phonons [15] and optomechanically induced amplification [16]. By combining the BS and TMS interactions, the Bogoliubov mode in the optomechanical system can be generated [17–19]. The back-action evasion measurement for the mechanical quadrature component was achieved when the coupling strengths of the BS and TMS interactions were equal [20–23]. Moreover, the quantum squeezed state of the mechanical mode has been generated by increasing the coupling strength of the BS interaction to be larger than that of the TMS interaction [18,24–28].

Squeezed light fields are typical nonclassical states where the fluctuation noise in one quadrature of the optical field is below the standard quantum noise limit; these fields have been demonstrated in optomechanical systems [29–31]. The two-mode squeezed state is a special type of quantum entangled state, where the amplitude quadrature and phase quadrature of the states are both quantum correlated. Quantum entanglement is a crucial resource for quantum communication and quantum computing [32,33], can improve measurement sensitivity, and is beneficial to quantum metrology [34,35]. The quantum entanglement of two output optical fields in optomechanical systems has been investigated by coupling a cavity mode with a mechanical mode [36,37], two cavity modes simultaneously with a mechanical mode [38–40], or two mechanical modes [41,42].

In this study, we present a scheme to produce strong quantum entanglement via the controllable four-wave-mixing (FWM) process in a single-cavity, weak-coupling optomechanical system. Our scheme requires neither the strong coupling condition nor multiple cavity modes. Instead, only a two-tone pump field [43–45] is required, which couples with the mechanical resonator to generate the desired BS and TMS interactions. In this way, the effective susceptibility of the optomechanical cavity is modified, and an optomechanically FWM process is induced when a weak signal field is incident on the system.

The FWM enables a significant amplification of the signal field and generates an associated FWM field. We find that there exists strong quantum entanglement between the signal and the FWM fields with realistic experimental parameters. Our scheme works in a resolved-sideband regime, which facilitates the high-efficiency laser cooling of the mechanical mode, a key factor for achieving strong quantum entanglement for optomechanical systems. We show that even without the strong optomechanical coupling, considerable quantum entanglement at room temperature can still be achieved by carefully controlling the ratio of BS and TMS interactions.

*yongmin@sxu.edu.cn

The rest of this study is organized as follows: In Sec. II, we present the theoretical model of the optomechanical system and derive the output field, which consists of the classical mean field and quantum fluctuation field, by solving the quantum Langevin equation. In Sec. III, we investigate the classical characteristics of the signal and FWM fields, including the bandwidth, center frequency, and intensity gain. In Sec. IV, we study the quantum entanglement between the signal and FWM fields, and analyze the dependence of the entanglement on the relevant experimental parameters, including the optomechanical coupling strength, escape efficiency of the optical cavity, and environmental temperature. Finally, conclusions are given in Sec. V.

II. OPTOMECHANICAL SYSTEM MODEL

A. Hamiltonian and Langevin equations

We consider an optomechanical system consisting of a mechanical resonator with resonance frequency ω_m and an optical cavity with intrinsic resonance frequency ω_{c0}. The optical cavity is driven by an intense two-tone pump field consisting of a redshifted sideband $\omega_- = \omega_c - \omega_0$, a blueshifted sideband $\omega_+ = \omega_c + \omega_0$, and a weak probe field with frequency ω_s. Here, ω_c is the effective resonance frequency of the optical cavity considering the average radiation pressure of the two-tone pump field. As we will show below, in the resolved-sideband regime $\kappa \ll \omega_m$ and under the rotating-wave approximation, the optomechanical coupling of the redshifted and blueshifted sidebands with the mechanical resonator produce the BS interaction and TMS interaction, respectively [46,47].

The Hamiltonian of the optomechanical system is written as

$$H = \hbar\omega_{c0}a^\dagger a + \hbar\omega_m b^\dagger b + \hbar g_0 a^\dagger a(b^\dagger + b) + H_{\rm drive}, \quad (1)$$

where $a(b)$ is the photon (phonon) annihilation operator, and g_0 denotes the single-photon optomechanical coupling strength. The first two terms on the right-hand side of Eq. (1) are the free Hamiltonian of the cavity field and the mechanical mode, respectively. The third term is the interaction Hamiltonian, and $H_{\rm drive}$ denotes the driving Hamiltonian, which is written as

$$H_{\rm drive} = i\hbar\sqrt{\kappa_{ex}}(\alpha_+ e^{-i\omega_+ t} + \alpha_- e^{-i\omega_- t} + \alpha_s e^{-i\omega_s t})a^\dagger + \text{H.c.}, \quad (2)$$

where κ_{ex} is the decay rate of the input cavity mirror (external loss rate), and κ_0 is the internal loss rate of the cavity apart from κ_{ex}, which results in a total decay rate $\kappa = \kappa_{ex} + \kappa_0$. The driving strength $|\alpha_\mu| = \sqrt{P_\mu/\hbar\omega_\mu}(\mu = \pm, s)$ is related to the input laser power P_μ, and we assume that $|\alpha_+|, |\alpha_-| \gg |\alpha_s|$.

The quantum Langevin equations of the cavity field a and mechanical mode b have the forms

$$\dot{a} = -(i\omega_{c0} + \kappa/2)a - ig_0 a(b + b^\dagger) + \sqrt{\kappa_{ex}}\varepsilon(t) + \sqrt{\kappa_{ex}}a_{\rm in} + \sqrt{\kappa_0}a_v, \quad (3)$$

$$\dot{b} = -(i\omega_m + \gamma_m/2)b - ig_0 a^\dagger a + \sqrt{\gamma_m}\eta, \quad (4)$$

where $\varepsilon(t) = \alpha_+ e^{-i\omega_+ t} + \alpha_- e^{-i\omega_- t} + \alpha_s e^{-i\omega_s t}$ denotes the total driving fields, and $a_{\rm in}$ and a_v denote the quantum fluctuation noise of the input field and vacuum field, respectively. γ_m is the intrinsic mechanical damping rate, and η is the thermal drive to the mechanical resonator.

We apply the transformations $a = \bar{\alpha}_- e^{-i\omega_- t} + \bar{\alpha}_+ e^{-i\omega_+ t} + a_1$ and $b = \bar{\beta} + b_1$ to the optical field and mechanical mode, where a_1 and b_1 represent the fluctuation fields of the cavity mode a and mechanical mode b, respectively, and $\bar{\alpha}_\pm = \sqrt{\kappa_{ex}}\alpha_\pm/(\mp i\omega_0 + \kappa/2)$ represents the mean intracavity coherent amplitude of the two-tone pump field. Without loss of generality, we assume $\bar{\alpha}_\pm$ to be real in the following. Note that the intrinsic resonance frequency of the optical cavity ω_{c0} is shifted to $\omega_c = \omega_{c0} + g_0\bar{x}$ by the average displacement of the mechanical mode, which is given by $\bar{x} = \bar{\beta} + \bar{\beta}^* = -2g_0(\bar{\alpha}_-^2 + \bar{\alpha}_+^2)/\omega_m$.

In the resolved-sideband regime $\kappa \ll \omega_m$, by transforming the system to a rotating frame defined by $H_0 = \hbar\omega_c a_1^\dagger a_1 + \hbar\omega_0 b_1^\dagger b_1$ and applying a rotating-wave approximation, the linearized interaction Hamiltonian can be written as follows by neglecting the nonlinear terms:

$$H = \hbar\Delta_m b_1^\dagger b_1 + \hbar G_-(a_1^\dagger b_1 + a_1 b_1^\dagger) + \hbar G_+(a_1^\dagger b_1^\dagger + a_1 b_1), \quad (5)$$

where $\Delta_m = \omega_m - \omega_0$ denotes the mechanical frequency detuning between the intrinsic mechanical frequency ω_m and the frequency ω_0, and $G_- = g_0\bar{\alpha}_-$ ($G_+ = g_0\bar{\alpha}_+$) denotes the optomechanical coupling strength of the BS (TMS) interaction arising from the redshifted (blueshifted) sideband. Starting with Eq. (5), the quantum Langevin equations of the fluctuation fields a_1 and b_1 are given by

$$\dot{a}_1 = (-\kappa/2)a_1 - i(G_- b_1 + G_+ b_1^\dagger) + \sqrt{\kappa_{ex}}\alpha_s e^{-i\Delta_s t} + \sqrt{\kappa_{ex}}a_{\rm in} + \sqrt{\kappa_0}a_v, \quad (6)$$

$$\dot{b}_1 = -(i\Delta_m + \gamma_m/2)b_1 - i(G_- a_1 + G_+ a_1^\dagger) + \sqrt{\gamma_m}\eta, \quad (7)$$

where $\Delta_s = \omega_s - \omega_c$ is the frequency difference between the signal field frequency ω_s and the effective resonance frequency of the optical cavity ω_c.

B. Solutions in the frequency domain

To facilitate the characterization of the entanglement properties of specific spectral components in Sec. IV, we use the windowed Fourier transform $o[\omega] = \lim_{\tau\to\infty}(1/\sqrt{\tau})\int_{-\tau/2}^{+\tau/2} o(t)e^{i\omega t}dt$ [1,48,49] instead of the conventional Fourier transform with the range of time integration from $-\infty$ to $+\infty$, where τ is the finite sampling time. In this case, $o[\omega]$ are discrete bosonic operators satisfying the commutation relation $[o[\omega], o[\omega']^\dagger] = \delta_{\omega\omega'}$ [48], in contrast to the continuous field bosonic operators with $[o[\omega], o[\omega']^\dagger] = \delta(\omega - \omega')$. By converting Eqs. (6) and (7) into the frequency domain using the Fourier transform, we obtain the corresponding optomechanical damping rate $\gamma_{\rm opt}$ and mechanical frequency shift $\delta\omega_m$ [1] in the weak-coupling regime $G_\pm \ll \kappa$ (see Appendix A for details):

$$\gamma_{\rm opt} = \frac{\kappa(G_-^2 - G_+^2)}{\Delta_m^2 + \kappa^2/4}, \quad (8)$$

$$\delta\omega_m = \frac{\Delta_m(G_-^2 - G_+^2)}{\Delta_m^2 + \kappa^2/4}. \quad (9)$$

Considering the input-output relation $a_{\rm out}[\omega] = -a_{\rm in}[\omega] + \sqrt{\kappa_{ex}}a_1[\omega]$, the reflective field from the optical cavity is given by

$$\begin{aligned} a_r[\omega] = {} & (A[\omega]\kappa_{ex} - 1)(\alpha_s[\omega - \Delta_s] + a_{\rm in}[\omega]) \\ & + A[\omega]\sqrt{\kappa_{ex}\kappa_0}a_v[\omega] + B[\omega]\kappa_{ex}(\alpha_s^*[\omega + \Delta_s] \\ & + a_{\rm in}^\dagger[\omega]) + B[\omega]\sqrt{\kappa_{ex}\kappa_0}a_v^\dagger[\omega] + C[\omega]\sqrt{\kappa_{ex}\gamma_m}\eta[\omega] \\ & + D[\omega]\sqrt{\kappa_{ex}\gamma_m}\eta^\dagger[\omega]. \end{aligned} \tag{10}$$

The reflective field $a_r[\omega]$ consists of two parts: the classical mean field α_r and the quantum fluctuation field a_{r1}, which are expressed by

$$\alpha_r[\omega] = (A[\omega]\kappa_{ex} - 1)\alpha_s[\omega - \Delta_s] + B[\omega]\kappa_{ex}\alpha_s^*[\omega + \Delta_s], \tag{11}$$

$$\begin{aligned} a_{r1}[\omega] = {} & (A[\omega]\kappa_{ex} - 1)a_{\rm in}[\omega] + A[\omega]\sqrt{\kappa_{ex}\kappa_0}a_v[\omega] \\ & + B[\omega]\kappa_{ex}a_{\rm in}^\dagger[\omega] + B[\omega]\sqrt{\kappa_{ex}\kappa_0}a_v^\dagger[\omega] \\ & + C[\omega]\sqrt{\kappa_{ex}\gamma_m}\eta[\omega] + D[\omega]\sqrt{\kappa_{ex}\gamma_m}\eta^\dagger[\omega]. \end{aligned} \tag{12}$$

From Eqs. (11) and (12), it is clear that the optomechanical interaction mechanism modifies the susceptibility of the optical cavity from its original form $\chi_c[\omega]$ and induces a conjugate field $\alpha_s^*[\omega + \Delta_s]$ (FWM field). The modified susceptibility of the optical cavity depends on the coefficients $A[\omega]$, $B[\omega]$, $C[\omega]$, and $D[\omega]$, which in turn rely on the parameters of the optomechanical system (see Appendix A for details).

III. OPTOMECHANICAL FWM PROCESS

In this section, we investigate the frequency response characteristics of the classical field. Assuming that the input signal field α_s is a monochromatic field and transforming Eq. (11) into the time domain, we find that there are two frequency components $\omega = \Delta_s$ and $\omega = -\Delta_s$ in the reflective classical field $\alpha_r[\omega]$:

$$\alpha_{r-s}[\Delta_s] = (A[\Delta_s]\kappa_{ex} - 1)\alpha_s, \tag{13}$$

$$\alpha_{r-c}[-\Delta_s] = B[-\Delta_s]\kappa_{ex}\alpha_s^*, \tag{14}$$

where $\alpha_{r-s}[\Delta_s]$ and $\alpha_{r-c}[-\Delta_s]$ correspond to the signal and FWM fields ($\omega_F = 2\omega_c - \omega_s$), respectively, as shown in Fig. 1. From the above equations, the intensity gains of the reflective signal and FWM fields are

$$R_s[\Delta_s] = |\alpha_{r-s}[\Delta_s]/\alpha_s|^2 = |A[\Delta_s]\kappa_{ex} - 1|^2, \tag{15}$$

$$R_c[-\Delta_s] = |\alpha_{r-c}[-\Delta_s]/\alpha_s^*|^2 = |B[-\Delta_s]\kappa_{ex}|^2. \tag{16}$$

Figure 2 plots the intensity gain $R_s[\Delta_s]$ ($R_c[-\Delta_s]$) of the signal (FWM) field as a function of the frequency detuning Δ_s. The simulation parameters we use are $\omega_m = 2\pi \times 5.85 \times 10^5$ Hz, $\gamma_m = 2\pi \times 5$ Hz, $\kappa = 0.1\omega_m$, $\kappa_{ex} = 0.98\kappa$, and $\omega_0 = 0.95\omega_m$. The curves in Fig. 2 correspond to the TMS interaction coupling strengths of $G_+ = \{30070, 30000, 29900\}$ Hz from top to bottom, respectively, in which the BS interaction strength is set as $G_- = 3 \times 10^4$ Hz. For all curves, the weak-coupling condition $G_\pm \ll \kappa$ is satisfied. The signal (FWM) field presents a supernarrow frequency response

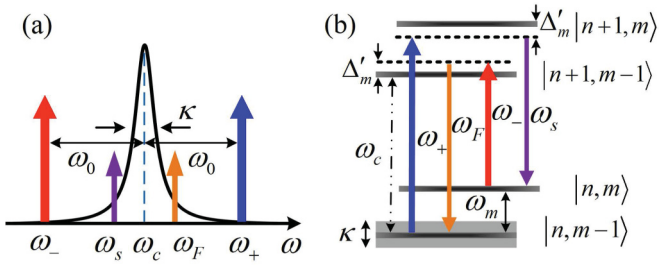

FIG. 1. (a) Spectrum of cavity response, optical driving fields, and FWM fields. ω_c: effective cavity resonance frequency; ω_- and ω_+: two-tone driving field; ω_s: signal field; ω_F: FWM field. (b) Energy-level diagram of the optomechanical system. Δ'_m is the effective mechanical detuning; m and n denote the phonon number of the mechanical mode and the photon number of the cavity mode, respectively.

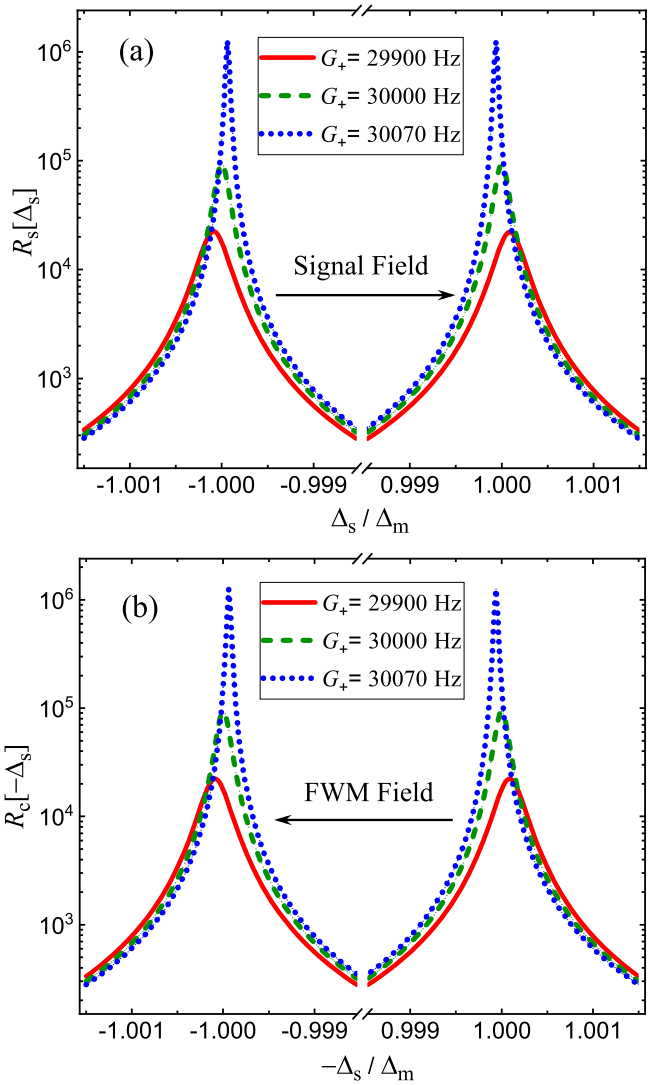

FIG. 2. Intensity gain spectrum of the reflective field versus the signal frequency detuning Δ_s for different coupling strengths G_+: (a) signal field and (b) FWM field. G_- is set as 3×10^4 Hz.

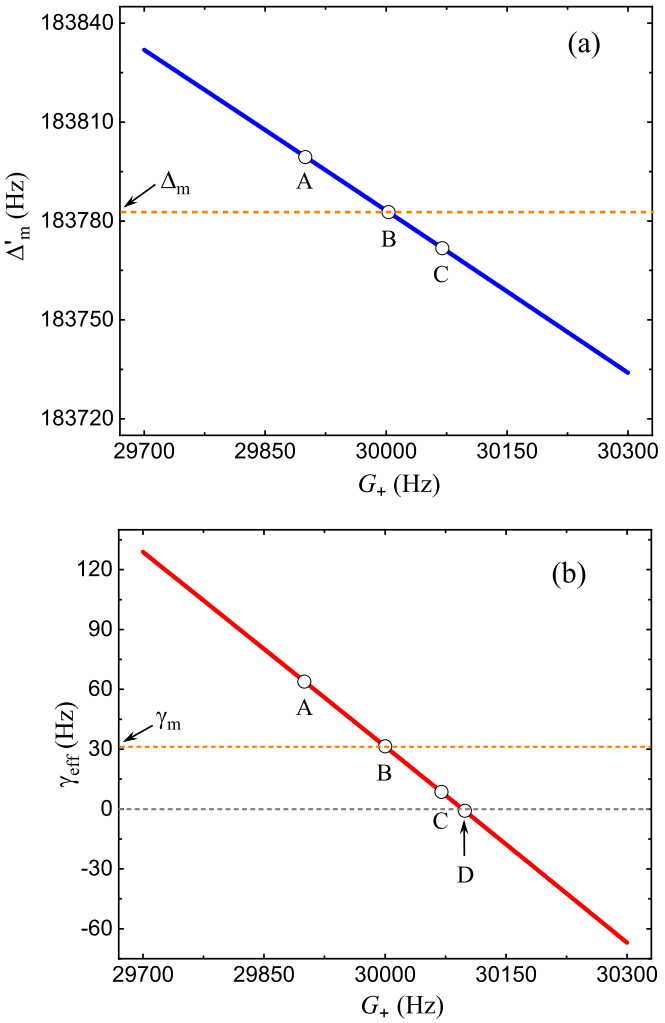

FIG. 3. (a) Effective mechanical frequency detuning Δ'_m and (b) effective damping rate $\gamma_{\rm eff}$ as a function of the TMS interaction strength G_+. For all cases, $G_- = 3 \times 10^4$ Hz.

bandwidth determined by the mechanical effective damping rate $\gamma_{\rm eff} = \gamma_m + \gamma_{\rm opt}$. The peak intensity gain of the signal (FWM) field occurs at the frequency of $\Delta_s = \mp\Delta'_m$ ($-\Delta_s = \pm\Delta'_m$), which indicates that injection of the weak signal field with frequency $\Delta_s = \mp\Delta'_m$ into the optomechanical system induces a FWM field with frequency $-\Delta_s = \pm\Delta'_m$ when the strong two-tone pump field is applied, as shown in Fig. 1(b). Note that $\Delta'_m = \Delta_m + \delta\omega_m$ denotes the effective mechanical frequency detuning, considering the mechanical frequency shift induced by the optomechanical self-energy [see Eq. (9)].

The frequency response characteristics of the FWM process is tunable by varying the optomechanical self-energy. In Fig. 3, we plot the effective mechanical frequency detuning Δ'_m and effective damping rate $\gamma_{\rm eff}$ as a function of the coupling strength G_+. Other simulation parameters are the same as those in Fig. 2. The circles A, B, and C represent three different G_+ in Fig. 2 with A :$G_+ = 29900$ Hz, B :$G_+ = 30000$ Hz, and C :$G_+ = 30070$ Hz. Note that the TMS interaction strength should satisfy $G_+ < 30100$ Hz (point D) to avoid the instability effect of the mechanical system.

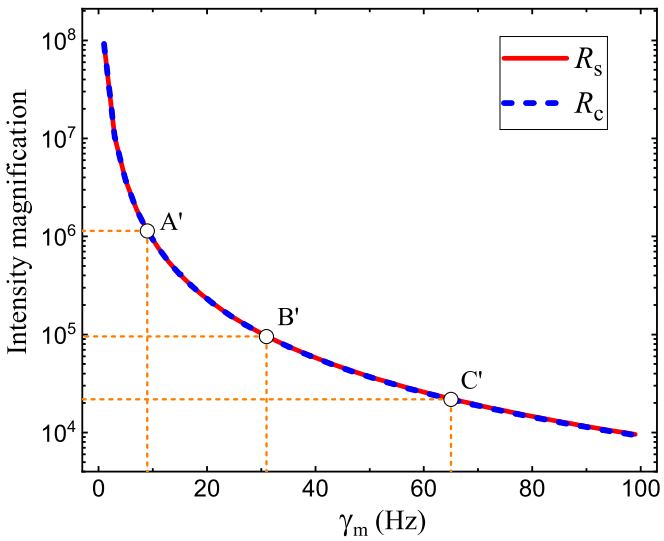

FIG. 4. Intensity gain of the signal and FWM fields as a function of the mechanical intrinsic damping rate γ_m.

From Eqs. (15) and (16), the peak intensity gain of the signal (FWM) field at the center frequency $\Delta_s = -\Delta'_m$ ($-\Delta_s = \Delta'_m$) is given by

$$R_s = |A[-\Delta'_m]\kappa_{ex} - 1|^2, \tag{17}$$

$$R_c = |B[\Delta'_m]\kappa_{ex}|^2. \tag{18}$$

Figure 4 shows the peak intensity gain of the signal (FWM) field as a function of the mechanical intrinsic damping rate γ_m, in which the optomechanical self-energy is set to zero, that is, $G_+ = G_- = 3 \times 10^4$ Hz, and the other simulation parameters are the same as those in Fig. 2. We find that the lower mechanical intrinsic damping rate γ_m makes a higher intensity gain, which can exceed 10^5 at the region of $\gamma_m < 30$ Hz. This indicates that a high-quality factor of the mechanical resonator predicts a high intensity gain in the absence of optomechanical self-energy.

For a given mechanical resonator with a fixed quality factor, one can tune the peak intensity gain by controlling the optomechanical self-energy. To this end, we fix G_- and adjust G_+ to 29900 Hz (point A), 30000 Hz (point B), and 30070 Hz (point C), as shown in Fig. 3(b); the effective mechanical damping rate is changed to $\gamma_{\rm eff} = \{64.0, 31.4, 8.5\}$ Hz. In order to verify that the effective mechanical damping $\gamma_{\rm eff}$ has the same tuning effect on the intensity gain as the intrinsic damping rate γ_m, we extract three intrinsic damping rates: A′ : 8.5 Hz, B′ : 31.4 Hz, and C′ : 64.0 Hz. These are presented in Fig. 4, and have the same values as A, B, and C. We find that the intensity gains of A′, B′, andC′ in Fig. 4 are equal to the peak gains of A, B, and C, respectively (see Fig. 2). According to the above analysis, the peak gain of the intensity mainly depends on the effective mechanical damping rate when the TMS coupling strength G_+ varies around G_-.

IV. THE QUANTUM ENTANGLEMENT

In this section, we study the properties of quantum entanglement between the signal and FWM fields with logarithmic

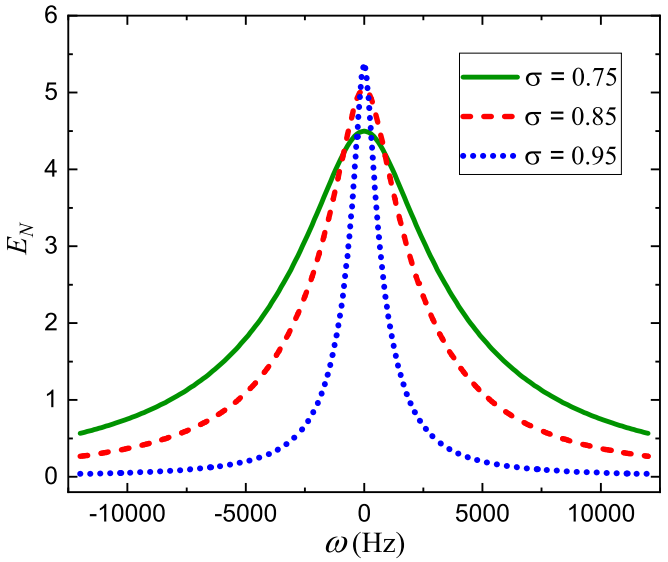

FIG. 5. Entanglement of the signal and FWM modes as a function of analysis frequency under different TMS interaction strengths G_+. $\sigma = G_+/G_-$ and $G_- = 1.2 \times 10^5$ Hz.

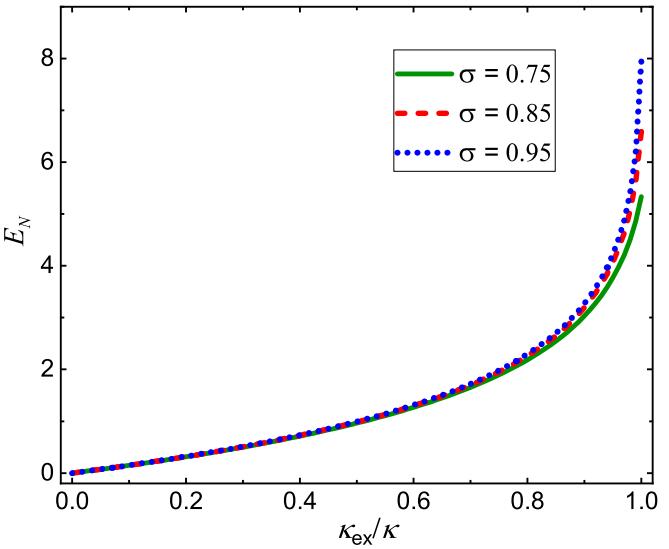

FIG. 6. The maximum entanglement at the center analysis frequency ($\omega = 0$) versus the escape efficiency of the optical cavity κ_{ex}/κ. For all curves, $G_- = 1.2 \times 10^5$ Hz.

negativity. For two-mode Gaussian states, the logarithmic negativity can be expressed as

$$E_N = \min\{0, -\log_2(2\nu_-)\}, \tag{19}$$

where the parameter ν_- is the smallest symplectic eigenvalues of the covariance matrix V charactering the state of the signal and FWM modes. The components of the covariance matrix V have the standard form $V_{ij} = (1/2)\langle \Delta\zeta_i \Delta\zeta_j + \Delta\zeta_j \Delta\zeta_i \rangle$, where $\Delta\zeta_i = \zeta_i - \langle \zeta_i \rangle$, $\vec{\zeta}_i = [X_s, Y_s, X_c, Y_c]$, and $X_s(Y_s)$ and $X_c(Y_c)$ are amplitude quadrature (phase quadrature) of the signal and FWM fields, respectviely. Note that for the spectral components of continuous stationary fields, the parameter ν_- is equal to the two-mode squeezing spectrum [48], $\nu_-[\omega] = S[\omega]$ (see Appendix B for detailed expressions of $S[\omega]$).

Figure 5 plots the entanglement of the signal and FWM modes as a function of analysis frequency under different TMS interaction strength G_+. The parameters of the mechanical resonator we use for simulation are taken from Ref. [50], with the mechanical frequency $\omega_m = 2\pi \times 1.14 \times 10^6$ Hz and the quality factor $Q_m = 1.03 \times 10^9$. The other simulation parameters used are $\kappa = 0.1\omega_m$, $\kappa_{ex} = 0.98\kappa$, $\omega_0 = 0.95\omega_m$, and the environment temperature $T = 1$ K. Note that $\omega = 0$ corresponds to the frequency of the peak intensity gain of the signal (FWM) field, $\Delta_s = -\Delta'_m$ ($-\Delta_s = \Delta'_m$) [Fig. 2(a)].

In order to satisfy the weak-coupling condition $G_\pm \ll \kappa$, we fix the coupling strength of the BS interaction $G_- = 1.2 \times 10^5$ Hz and vary the coupling strength of the TMS interaction G_+, which is normalized by G_-, that is, $\sigma = G_+/G_-$. The quantum entanglement increases with increasing σ (or TMS interaction strength G_+). For $\sigma = 0.95$, a strong quantum entanglement (∼5.3) can be achieved. However, the bandwidth of the noise power spectrum decreases when σ (G_+) increases; this is due to the effective mechanical damping rate being reduced [see Eq. (8)].

The achievable quantum entanglement also depended on other parameters of the optomechanical system, for instance, the escape efficiency of the optical cavity κ_{ex}/κ. Figure 6 plots the maximum quantum entanglement at the center analysis frequency ($\omega = 0$) as a function of the escape efficiency of the optical cavity κ_{ex}/κ; the other simulation parameters are the same as those in Fig. 5. We find that a higher escape efficiency is beneficial to achieving stronger quantum entanglement, and significant entanglement can be achieved for an escape efficiency κ_{ex}/κ larger than 0.9. In the range of $\kappa_{ex}/\kappa < 0.9$, the differences of the entanglement for three different ratios of optomechanical coupling strength, $\sigma = 0.75, 0.85, 0.95$, are not distinct.

The achievable quantum entanglement also depends on the environment temperature where the mechanical resonator is located. A large thermal phonon occupation number signifies intense thermal motion of the mechanical resonator, which modulates the optical fields in a noncoherent way and degrades the quantum entanglement of the optical fields. Usually, a mechanical resonator is precooled by a cryogenic cooling system to keep the optomechanical system away from thermal noises. Figure 7 plots the maximum quantum entanglement as a function of the environment temperature T. The optomechanical coupling strength ratio between the BS interaction G_- and TMS interaction G_+ is set to $\sigma = G_+/G_- = 0.95$, and G_- is varied (other parameters are the same as those in Fig. 5).

For three different BS interaction strengths G_-, Fig. 7 shows that the quantum entanglement decreases with the increasing environment temperature; that is, lower thermal phonon occupation is required to achieve a greater quantum entanglement. At finite temperature, the entanglement significantly depends on the BS interaction strength G_- and TMS interaction strength G_+. For the coupling strength $G_- = 1.2 \times 10^5$ Hz (green solid line), strong entanglement of ∼5.3 can be generated at $T = 1$ K and it drops with increasing temperature and disappears at room temperature ($T = 298$ K). When improving the coupling strength G_- to 1.8×10^5 Hz

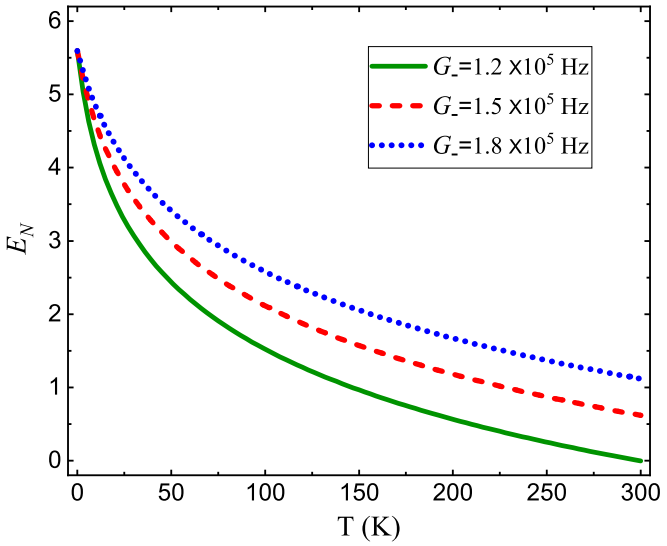

FIG. 7. Maximum entanglement at the center analysis frequency ($\omega = 0$) as a function of the environment temperature T with $\sigma = G_+/G_- = 0.95$.

(blue dotted line), quantum entanglement beyond 3 dB can still be obtained at room temperature, where the thermal phonons' occupation of the mechanical mode $\bar{n}_{th}$ is around 5.4×10^6. We see that our scheme is quite robust against temperature (thermal mechanical noise), and the robustness is more significant for stronger BS interaction and TMS interaction, which is particularly important for practical preparation of optical quantum entanglement.

In the above analysis, we have assumed that the two tone pumps are symmetrically detuned from the cavity resonance frequency for simplicity. In this case, the output signal and FWM fields are symmetrically located at two sides of the cavity resonance frequency. If the detuning of the two tone pumps are nonsymmetric with $\omega_- = \omega_c - \omega_0 + \Delta$ and $\omega_+ = \omega_c + \omega_0$, the simulations shows that output signal and FWM fields will also be nonsymmetric relative to the cavity resonance and their intensity gain decrease accordingly. For $\Delta = 5 \times 10^{-3}\omega_m$, which is feasible with current technology, the intensity gain is still above several hundreds. In this case, the entanglement is almost intact.

V. CONCLUSIONS

In summary, we have proposed a scheme to generate strong quantum entanglement by a controllable optomechanical FWM mechanism in a resolved-sideband and weak-coupling optomechanical system. First, we studied the classical behaviors of the optomechanical FWM process and showed that the frequency response characteristics, including the bandwidth, center frequency, and intensity gain, are tunable by the optomechanical self-energy effect. Then, we investigated the quantum entanglement characteristics between the signal and FWM fields, and found that the two optical fields are strongly quantum entangled with a logarithm negativity of ∼5.3 in proper conditions. We analyzed the key factors that affect the degree of the quantum entanglement and its bandwidth, including the optomechanical coupling strength (BS and TMS interactions) and their ratio, the escape efficiency of the optical cavity, and the initial environment temperature of the mechanical resonator. In particular, we find that significant entanglement with logarithm negativity larger than 1 can be achieved at room temperatures with the state-of-art optomechanical systems.

The presented scheme provides a promising way for quantum state engineering with low pump power, integrated microdevices. In principle, it can apply to various optomechanical and electromechanical systems operating from the ultraviolet to microwave band, which may find potential applications in future quantum communication network and quantum information processing.

ACKNOWLEDGMENT

This work is supported by the National Key R&D Program of China (Grant No. 2016YFA0301403), the National Natural Science Foundation of China (NSFC) (Grants No. 11774209 and No. 11804208), Key Research and Development Projects of Shanxi Province (201803D121065), and Shanxi 1331KSC.

APPENDIX A: SOLUTIONS OF THE LANGEVIN EQUATIONS IN THE FREQUENCY DOMAIN

Using the Fourier transform, Eqs. (6) and (7) are converted into the frequency domain:

$$a_1[\omega] = \chi_c[\omega]\{-i(G_- b_1[\omega] + G_+ b_1^\dagger[\omega]) + \sqrt{\kappa_{ex}}\alpha_s[\omega - \Delta_s] + \sqrt{\kappa_{ex}}a_{\rm in}[\omega] + \sqrt{\kappa_0}a_v[\omega]\}, \tag{A1}$$

$$b_1[\omega] = \chi_m[\omega]\{-i(G_- a_1[\omega] + G_+ a_1^\dagger[\omega]) + \sqrt{\gamma_m}\eta[\omega]\}, \tag{A2}$$

where $\chi_c[\omega] = (-i\omega + \kappa/2)^{-1}$ and $\chi_m[\omega] = [-i(\omega - \Delta_m) + \gamma_m/2]^{-1}$ are the susceptibilities of the optical cavity and mechanical resonator, respectively. Combining Eqs. (A1) and (A2), and using the operator conjugate relation $(o[\omega])^\dagger = o^\dagger[-\omega]$, we obtain the fluctuation field of the optical cavity mode in the frequency domain,

$$\begin{aligned} a_1[\omega] = {} & A[\omega](\sqrt{\kappa_{ex}}\alpha_s[\omega - \Delta_s] + \sqrt{\kappa_{ex}}a_{\rm in}[\omega] + \sqrt{\kappa_0}a_v[\omega]) \\ & + B[\omega](\sqrt{\kappa_{ex}}\alpha_s^*[\omega + \Delta_s] + \sqrt{\kappa_{ex}}a_{\rm in}^\dagger[\omega] + \sqrt{\kappa_0}a_v^\dagger[\omega]) \\ & + C[\omega]\sqrt{\gamma_m}\eta[\omega] + D[\omega]\sqrt{\gamma_m}\eta^\dagger[\omega]. \end{aligned} \tag{A3}$$

The coefficients that depend on the related parameters of the optomechanical system are given by

$$\begin{aligned} A[\omega] &= \frac{\chi_c[\omega]\{1 + \chi_c[\omega](G_-^2\chi_m^*[-\omega] - G_+^2\chi_m[\omega])\}}{(1 + \chi_m[\omega]\Sigma[\omega])(1 + \chi_m^*[-\omega]\Sigma[\omega])}, \\ B[\omega] &= \frac{\chi_c[\omega]\chi_c[\omega]G_-G_+(\chi_m^*[-\omega] - \chi_m[\omega])}{(1 + \chi_m[\omega]\Sigma[\omega])(1 + \chi_m^*[-\omega]\Sigma[\omega])}, \\ C[\omega] &= -i\frac{\chi_c[\omega]\chi_m[\omega]G_-}{(1 + \chi_m[\omega]\Sigma[\omega])}, \\ D[\omega] &= -i\frac{\chi_c[\omega]\chi_m^*[-\omega]G_+}{(1 + \chi_m^*[-\omega]\Sigma[\omega])}. \end{aligned} \tag{A4}$$

Here, $\Sigma[\omega]$ represents the optomechanical self-energy that is derived from the unequal optomechanical coupling strength between the BS and TMS interactions, and is defined as

$$\Sigma[\omega] = \chi_c[\omega](G_-^2 - G_+^2). \tag{A5}$$

The real and imaginary parts of the optomechanical self-energy correspond to the frequency-dependent optomechanical damping rate $\gamma_{\rm opt} = 2{\rm Re}(\Sigma[\omega])$ and mechanical frequency shift $\delta\omega_m[\omega] = {\rm Im}(\Sigma[\omega])$, respectively. In the weak-coupling regime $G_\pm \ll \kappa$, the corresponding optomechanical damping rate and mechanical frequency shift [1] are given by

$$\gamma_{\rm opt} = \frac{\kappa(G_-^2 - G_+^2)}{\Delta_m^2 + \kappa^2/4}, \tag{A6}$$

$$\delta\omega_m = \frac{\Delta_m(G_-^2 - G_+^2)}{\Delta_m^2 + \kappa^2/4}. \tag{A7}$$

APPENDIX B: THE QUANTUM CORRELATION SPECTRUM

In this appendix, the detailed expressions for the amplitude quadrature sum noise power spectrum $S_{XX}^{+}[\omega]$ and the phase quadrature difference noise power spectrum $S_{YY}^{-}[\omega]$ are derived. The amplitude and phase quadratures of the signal and FWM fields in the frequency domain are defined as

$$X_s[\omega] = (a_{r1}[\omega - \Delta_s] + a_{r1}^\dagger[\omega + \Delta_s])/\sqrt{2}, \tag{B1}$$

$$Y_s[\omega] = -i(a_{r1}[\omega - \Delta_s] - a_{r1}^\dagger[\omega + \Delta_s])/\sqrt{2}, \tag{B2}$$

$$X_c[\omega] = (a_{r1}[\omega + \Delta_s] + a_{r1}^\dagger[\omega - \Delta_s])/\sqrt{2}, \tag{B3}$$

$$Y_c[\omega] = -i(a_{r1}[\omega + \Delta_s] - a_{r1}^\dagger[\omega - \Delta_s])/\sqrt{2}. \tag{B4}$$

From the above optical field quadratures, we further define two combined field quadratures, including both signal and FWM fields. These are written as

$$X^{+}[\omega] = (X_s[\omega] + X_c[\omega])/\sqrt{2}, \tag{B5}$$

$$Y^{-}[\omega] = (Y_s[\omega] - Y_c[\omega])/\sqrt{2}. \tag{B6}$$

The amplitude quadrature sum noise power spectrum $S_{XX}^{+}[\omega]$ and the phase quadrature difference noise power spectrum $S_{YY}^{-}[\omega]$ have the following form:

$$S_{XX}^{+}[\omega] = \big(S_{XX}^{s-s}[\omega] + S_{XX}^{c-c}[\omega] + S_{XX}^{s-c}[\omega] + S_{XX}^{c-s}[\omega]\big)/2, \tag{B7}$$

$$S_{YY}^{-}[\omega] = \big(S_{YY}^{s-s}[\omega] + S_{YY}^{c-c}[\omega] - S_{YY}^{s-c}[\omega] - S_{YY}^{c-s}[\omega]\big)/2. \tag{B8}$$

From the right-hand sides of Eqs. (B7) and (B8), we note that the quantum correlation noise power spectrum contains four terms. The first two terms represent the self-correlation spectrum of the signal (FWM) field and itself, and the last two terms are derived from the cross-correlation spectra between the signal and FWM fields, which are essential to generate the quantum entanglement.

From Eq. (12) presented in Sec. II, the Fourier transform of the conjugate of the fluctuation field a_{r1} is given by

$$\begin{aligned} a_{r1}^\dagger[\omega] = {} & M[\omega]\kappa_{ex}a_{\rm in}[\omega] + M[\omega]\sqrt{\kappa_{ex}\kappa_0}a_v[\omega] \\ & + (N[\omega]\kappa_{ex} - 1)a_{\rm in}^\dagger[\omega] + N[\omega]\sqrt{\kappa_{ex}\kappa_0}a_v^\dagger[\omega] \\ & + P[\omega]\sqrt{\kappa_{ex}\gamma_m}\eta[\omega] + Q[\omega]\sqrt{\kappa_{ex}\gamma_m}\eta^\dagger[\omega], \end{aligned} \tag{B9}$$

where the related coefficients are

$$\begin{aligned} M[\omega] &= \frac{\chi_c[\omega]\chi_c[\omega]G_-G_+(\chi_m[\omega] - \chi_m^*[-\omega])}{(1 + \chi_m[\omega]\Sigma[\omega])(1 + \chi_m^*[-\omega]\Sigma[\omega])}, \\ N[\omega] &= \frac{\chi_c[\omega]\{1 + \chi_c[\omega](G_-^2\chi_m[\omega] - G_+^2\chi_m^*[-\omega])\}}{(1 + \chi_m[\omega]\Sigma[\omega])(1 + \chi_m^*[-\omega]\Sigma[\omega])}, \\ P[\omega] &= i\frac{\chi_c[\omega]\chi_m[\omega]G_+}{(1 + \chi_m[\omega]\Sigma[\omega])}, \\ Q[\omega] &= i\frac{\chi_c[\omega]\chi_m^*[-\omega]G_-}{(1 + \chi_m^*[-\omega]\Sigma[\omega])}. \end{aligned} \tag{B10}$$

To derive the quadrature noise power spectrum, the following correlation relations are used, including the correlation of input optical fields, and thermal noise correlation of the mechanical mode in the frequency domain; here we have assumed that the input field modes are in coherent states:

$$\begin{aligned} \langle a_{\rm in}[\omega]a_{\rm in}^\dagger[\omega']\rangle &= \langle a_v[\omega]a_v^\dagger[\omega']\rangle = \delta_{-\omega\omega'}, \\ \langle a_{\rm in}^\dagger[\omega]a_{\rm in}[\omega']\rangle &= \langle a_v^\dagger[\omega]a_v[\omega']\rangle = 0, \\ \langle \eta[\omega]\eta^\dagger[\omega']\rangle &= (\bar{n}_{th} + 1)\delta_{-\omega\omega'}, \\ \langle \eta^\dagger[\omega]\eta[\omega']\rangle &= \bar{n}_{th}\delta_{-\omega\omega'}, \end{aligned} \tag{B11}$$

where $\bar{n}_{th}$ denotes the initial thermal phonons' occupation of the mechanical mode; it is proportional to the environment temperature where the mechanical resonator is located. Using Eqs. (12), (A4), and (B9)–(B11), we finally obtain

$$\begin{aligned} S_{XX}^{s-s}[\omega] = S_{YY}^{s-s}[\omega] = 0.5\{ & (A[\omega_1]\kappa_{ex} - 1)(N[-\omega_1]\kappa_{ex} - 1) + M[\omega_2]B[-\omega_2]\kappa_{ex}^2 + (A[\omega_1]N[-\omega_1] + M[\omega_2]B[-\omega_2])\kappa_{ex}\kappa_0 \\ & + \kappa_{ex}\gamma_m[(C[\omega_1]Q[-\omega_1] + P[\omega_2]Q[-\omega_2])(\bar{n}_{th} + 1) + (D[\omega_1]P[-\omega_1] + Q[\omega_2]C[-\omega_2])\bar{n}_{th}]\}, \end{aligned} \tag{B12}$$

$$\begin{aligned} S_{XX}^{c-c}[\omega] = S_{YY}^{c-c}[\omega] = 0.5\{ & (A[\omega_2]\kappa_{ex} - 1)(N[-\omega_2]\kappa_{ex} - 1) + M[\omega_1]B[-\omega_1]\kappa_{ex}^2 + (A[\omega_2]N[-\omega_2] + M[\omega_1]B[-\omega_1])\kappa_{ex}\kappa_0 \\ & + \kappa_{ex}\gamma_m[(C[\omega_2]P[-\omega_2] + P[\omega_1]Q[-\omega_1])(\bar{n}_{th} + 1) + (D[\omega_2]P[-\omega_2] + Q[\omega_1]C[-\omega_1])\bar{n}_{th}]\}, \end{aligned} \tag{B13}$$

$$\begin{aligned} S_{XX}^{s-c}[\omega] = -S_{YY}^{s-c}[\omega] = 0.5\{ & [(A[\omega_1]\kappa_{ex} - 1)B[-\omega_1] + M[\omega_2](N[-\omega_2]\kappa_{ex} - 1)]\kappa_{ex} + (A[\omega_1]B[-\omega_1] + M[\omega_2]N[-\omega_2])\kappa_{ex}\kappa_0 \\ & + \kappa_{ex}\gamma_m[(C[\omega_1]D[-\omega_1] + P[\omega_2]Q[-\omega_2])(\bar{n}_{th} + 1) + (D[\omega_1]C[-\omega_1] + Q[\omega_2]P[-\omega_2])\bar{n}_{th}]\}, \end{aligned} \tag{B14}$$

$$S_{XX}^{c-s}[\omega] = -S_{YY}^{c-s}[\omega] = 0.5\{[(A[\omega_2]\kappa_{ex} - 1)B[-\omega_2] + M[\omega_1](N[-\omega_1]\kappa_{ex} - 1)]\kappa_{ex} + (A[\omega_2]B[-\omega_2] + M[\omega_1]N[-\omega_1])\kappa_{ex}\kappa_0 + \kappa_{ex}\gamma_m[(C[\omega_2]D[-\omega_2] + P[\omega_1]Q[-\omega_1])(\bar{n}_{th} + 1) + (D[\omega_2]C[-\omega_2] + Q[\omega_1]P[-\omega_1])\bar{n}_{th}]\}, \quad \text{(B15)}$$

where $\omega_1 = \omega - \Delta_s$ and $\omega_2 = \omega + \Delta_s$.

Inserting Eqs. (B12)–(B15) into Eqs. (B7) and (B8), we obtain the quantum correlation spectrum between the signal and FWM fields. Note that $S_{XX}^{+}[\omega] = S_{YY}^{-}[\omega] = S[\omega]$; that is, the two-mode correlation is symmetric.

[1] M. Aspelmeyer, T. J. Kippenberg, and F. Marquardt, Rev. Mod. Phys. **86**, 1391 (2014).
[2] F. Marquardt, J. P. Chen, A. A. Clerk, and S. M. Girvin, Phys. Rev. Lett **99**, 093902 (2007).
[3] T. Rocheleau, T. Ndukum, C. Macklin, J. B. Hertzberg, A. A. Clerk, and K. C. Schwab, Nature (London) **463**, 72 (2010).
[4] J. D. Teufel, T. Donner, D. Li, J. W. Harlow, M. S. Allman, K. Cicak, A. J. Sirois, J. D. Whittaker, K. W. Lehnert, and R. W. Simmonds, Nature (London) **475**, 359 (2011).
[5] J. Chan, T. P. Mayer Alegre, A. H. Safavi-Naeini, J. T. Hill, A. Krause, S. Gröblacher, M. Aspelmeyer, and O. Painter, Nature (London) **478**, 89 (2011).
[6] A. H. Safavi-Naeini, J. Chan, J. T. Hill, T. P. M. Alegre, A. Krause, and O. Painter, Phys. Rev. Lett. **108**, 033602 (2012).
[7] R. W. Peterson, T. P. Purdy, N. S. Kampel, R. W. Andrews, P.-L. Yu, K. W. Lehnert, and C. A. Regal, Phys. Rev. Lett **116**, 063601 (2016).
[8] V. Fiore, Y. Yang, M. C. Kuzyk, R. Barbour, L. Tian, and H. Wang, Phys. Rev. Lett **107**, 133601 (2011).
[9] Y.-D. Wang and A. A. Clerk, Phys. Rev. Lett **108**, 153603 (2012).
[10] L. Tian, Phys. Rev. Lett **108**, 153604 (2012).
[11] E. Verhagen, S. Deléglise, S. Weis, A. Schliesser, and T. J. Kippenberg, Nature (London) **482**, 63 (2012).
[12] T. A. Palomaki, J. W. Harlow, J. D. Teufel, R. W. Simmonds, and K. W. Lehnert, Nature (London) **495**, 210 (2013).
[13] S. Weis, R. Rivière, S. Deléglise, E. Gavartin, O. Arcizet, A. Schliesser, and T. J. Kippenberg, Science **330**, 1520 (2010).
[14] A. H. Safavi-Naeini, T. P. M. Alegre, J. Chan, M. Eichenfield, M. Winger, Q. Lin, J. T. Hill, D. E. Chang, and O. Painter, Nature (London) **472**, 69 (2011).
[15] T. A. Palomaki, J. D. Teufel, R. W. Simmonds, and K. W. Lehnert, Science **342**, 710 (2013).
[16] F. Massel, T. T. Heikkilä, J.-M. Pirkkalainen, S. U. Cho, H. Saloniemi, P. J. Hakonen, and M. A. Sillanpää, Nature (London) **480**, 351 (2011).
[17] C. Dong, V. Fiore, M. C. Kuzyk, and H. Wang, Science **338**, 1609 (2013).
[18] A. Kronwald, F. Marquardt, and A. A. Clerk, Phys. Rev. A **88**, 063833 (2013).
[19] C. Dong, J. Zhang, V. Fiore, and H. Wang, Optica **1**, 425 (2014).
[20] A. A. Clerk, F. Marquadt, and K. Jacobs, New J. Phys. **10**, 095010 (2008).
[21] J. B. Hertzberg, T. Rocheleau, T. Ndukum, M. Savva, A. A. Clerk, and K. C. Schwab, Nat. Phys. **6**, 213 (2010).
[22] J. Suh, A. J. Weinstein, C. U. Lei, E. E. Wollman, S. K. Steinke, P. Meystre, A. A. Clerk, and K. C. Schwab, Science **344**, 1262 (2014).
[23] D. Malz and A. Nunnenkamp, Phys. Rev. A **94**, 053820 (2016).
[24] E. E. Wollman, C. U. Lei, A. J. Weinstein, J. Suh, A. Kronwald, F. Marquardt, A. A. Clerk, and K. C. Schwab, Science **349**, 952 (2015).
[25] F. Lecocq, J. B. Clark, R. W. Simmonds, J. Aumentado, and J. D. Teufel, Phys. Rev. X **5**, 041037 (2015).
[26] J.-M. Pirkkalainen, E. Damskägg, M. Brandt, F. Massel, and M. A. Sillanpää, Phys. Rev. Lett. **115**, 243601 (2015).
[27] C. U. Lei, A. J. Weinstein, J. Suh, E. E. Wollman, A. Kronwald, F. Marquardt, A. A. Clerk, and K. C. Schwab, Phys. Rev. Lett. **117**, 100801 (2016).
[28] X. You, Z.-Y. Li, and Y.-M. Li, Phys. Rev. A **96**, 063811 (2017).
[29] D. W. C. Brooks, T. Botter, S. Schreppler, T. P. Purdy, N. Brahms, and D. M. Stamper-Kurn, Nature (London) **488**, 476 (2012).
[30] T. P. Purdy, P.-L. Yu, R. W. Peterson, N. S. Kampel, and C. A. Regal, Phys. Rev. X. **3**, 031012 (2013).
[31] A. H. Safavi-Naeini, S. Gröblacher, J. H. Hill, J. Chan, M. Aspelmeyer, and O. Painter, Nature (London) **500**, 185 (2013).
[32] S. L. Braunstein and P. van Loock, Rev. Mod. Phys. **77**, 513 (2005).
[33] R. Horodecki, P. Horodecki, M. Horodecki, and K. Horodecki, Rev. Mod. Phys. **81**, 865 (2009).
[34] F. Hudelist, J. Kong, C. Liu, J. Jing, Z. Y. Ou, and W. Zhang, Nat. Commun. **5**, 3049 (2014).
[35] Y. Ma, H. Miao, B. H. Pang, M. Evans, C. Zhao, J. Harms, R. Schnabel, and Y. Chen, Nat. Phys. **13**, 776 (2017).
[36] C. Genes, A. Mari, P. Tombesi, and D. Vitali, Phys. Rev. A **78**, 032316 (2008).
[37] X.-h Yang, Z.-y Yin, and M. Xiao, Phys. Rev. A **99**, 013811 (2019).
[38] L. Tian, Phys. Rev. Lett. **110**, 233602 (2013).
[39] M. C. Kuzyk, S. J. van Enk, and H. Wang, Phys. Rev. A **88**, 062341 (2013).
[40] X. B. Yan, Z. J. Deng, X. D. Tian, and J. H. Wu, Opt. Express **27**, 24393 (2019).
[41] L. Zhou, Y. Han, J. T. Jing, and W. P. Zhang, Phys. Rev. A **83**, 052117 (2011).
[42] W. Ge, M. Al-Amri, H. Nha, and M. S. Zubairy, Phys. Rev. A **88**, 022338 (2013).
[43] A. Mari and J. Eisert, Phys. Rev. Lett. **103**, 213603 (2009).
[44] R. Garcés and G. J. de Valcárcel, Sci. Rep **6**, 21964 (2016).
[45] X. T. Zhang, J. T. Sheng, and H. B. Wu, Opt. Express **26**, 6285 (2018).
[46] A. M. Jayich, J. C. Sankey, B. M. Zwickl, C. Yang, J. D. Thompson, S. M. Girvin, A. A. Clerk, F. Marquardt, and J. G. E. Harris, New J. Phys. **10**, 095008 (2008).

[47] J. D. Thompson, B. M. Zwickl, A. M. Jayich, F. Marquardt, S. M. Girvin, and J. G. E. Harris, Nature (London) **452**, 72 (2008).

[48] S. Zippilli, G. D. Giuseppe, and D. Vitali, New J. Phys. **17**, 043025 (2015).

[49] A. A. Clerk, M. H. Devoret, S. M. Girvin, Florian Marquardt, and R. J. Schoelkopf, Rev. Mod. Phys. **82**, 1155 (2010).

[50] M. Rossi, D. Mason, J.-x. Chen, Y. Tsaturyan, and A. Schliesser, Nature (London) **563**, 53 (2018).